Effects of surface friction on a two-dimensional granular system: Cooling bound system

Meenakshi Dutt and R. P. Behringer
Department of Physics and Center of Nonlinear and Complex Systems, Duke University, Durham, North Carolina 27708-0305, USA
(Received 17 March 2004; published 13 December 2004)

Experiments performed by Painter and Behringer [Phys. Rev. E **62**, 2380 (2000)] on two-particle collisions and dynamics emphasized the importance of the role played by substrate friction, in particular kinetic friction, on the particle dynamics after collisions on a substrate. We present a numerical model which accounts for collisional and surface frictional dissipation and their influence on particle dynamics for a quasi-two-dimensional cooling initially dilute granular material. This model makes the simplifying assumption that the collision dynamics is determined solely by the incoming velocity and angular velocities of the colliding particles. We apply this model to a numerical simulation of a monolayer of monodisperse particles moving on a substrate, enclosed between inelastic walls. We find that surface friction—in particular, kinetic friction—plays a dominant role in determining the dynamics of quasi-two-dimensional multiparticle systems where the particles are in continuous contact with a substrate. Results from simulations performed for different system sizes indicate that surface friction and the inelastic walls lead to clustering of the particles in and near the vicinity of the walls. We find that the rate of decrease of average total kinetic energy is the highest when the majority of the particles have just collided and are experiencing kinetic frictional forces and torques. We also find from our calculations that, on average, particle-wall collisions lead to more dissipation than particle-particle collisions for a single particle for fixed restitutional parameters.

DOI: 10.1103/PhysRevE.70.061304 PACS number(s): 83.80.Fg

I. INTRODUCTION

In the past two decades, extensive experimental [1–17], theoretical, and numerical studies [18–34] (and others) on granular systems have been carried out. These studies have explored convection, clustering and collapse, velocity distributions, pattern formation [2,5–10] and granular cooling [3,4]. A number of the experiments were carried out with systems of spheres confined to or near a flat substrate. Here, the basic idea was that rolling friction is a very weak source of dissipation. Hence, if there is only rolling friction in an experimental system, there is an opportunity to experimentally probe the properties of cooling collisional systems.

The difficulty is that when two hard particles collide on a substrate, there is typically frictional frustration involving the contacts between the particles and the contacts of the particles with the substrate [18]. Except for very slow collisions, the frictional force between the particles exceeds that between the particles and substrate. As a consequence, one might expect that slipping of the particles is likely following a binary collision of particles on a substrate.

A number of theoretical and computational studies of collective granular dynamics have been conducted, but typically these do not include the effect of a substrate [if they are in two dimensions (2D)]. Among these are studies in s. [19,24,27,31]. Recent work by Kondic is an exception [23]. [However, in at least a few of the models [24,35], the coefficients of restitution represent energy and momentum losses when a collision occurs, so that effects from a substrate on the colliding particles might (in principle) be included in them.] However, there is no systematic study of which we are aware that considers the collective properties of relatively large numbers of particles moving on a substrate. The goal of this work and a companion paper [40] is to address this shortcoming.

Regarding friction between particles moving on a substrate, we note that two kinds of frictional forces are important: rolling and kinetic frictional forces. Rolling friction is quite weak, with a typical coefficient of friction $\mu_r \sim 10^{-3}$ [3,7] for hard spheres. Hence, it only gradually damps out particle motion. Kinetic friction acts on a particle when the instantaneous point of contact between the particle and substrate is not at rest. As noted, we expect that this situation may frequently arise immediately after a particle suffers a collision with another particle or a wall. In many cases, the normal contact force between the colliding particles is much stronger than the force of gravity; hence the frictional contacts between each of the particles and substrate give way, and slipping occurs (Fig. 1) [3]. The aim of the present study is to consider the simplest model that captures the key parts of the physics. Here, we are concerned with the strong damping that occurs when particles are sliding relative to the substrate as the result of a collision. This type of motion, which involves sliding friction, is associated with particle angular velocities that lie in the plane. The component of angular velocity in the vertical direction is also likely excited in typical collsions. A simple experiment, spinning a hard spherical particle on a flat surface, indicates that this type of motion is slowly damped. Therefore, we chose to focus on the components of rotational motion (the horizontal components). Previous studies [36–38] have looked at the dynamics of a rotating planar body or a sphere spinning vertically about its axis. This point shall be discussed in further detail.

The following estimate makes this more precise. Assuming for the moment a head-on collision, the interparticle contact force $F_{p\text{-}p}$ is the ratio of the impulse during contact between the two colliding particles Δp and the duration of the contact, τ_{con} ($\approx 10^{-5}$ s for steel spheres) [25]. Therefore, $F_{p\text{-}p} \sim \Delta p / \tau_{con}$, where $\Delta p \sim m(1+e)v$. The frictional force between a particle and the substrate is given by $F_{p\text{-}s} = \mu mg$

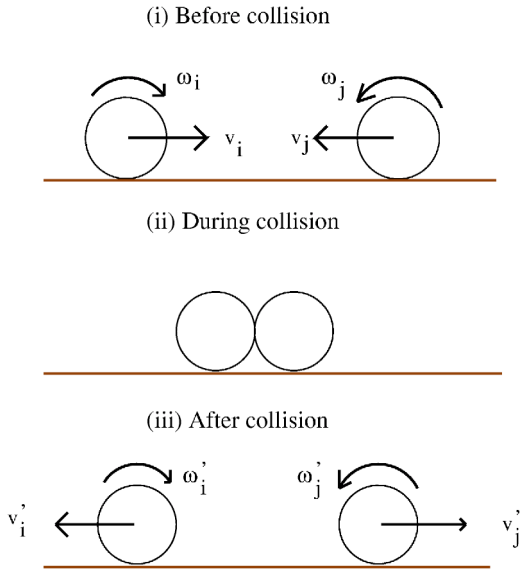

FIG. 1. Schematic diagram of *frictional frustration* during a two-particle collision process. (i) As particles roll towards each other, they experience (weak) rolling friction and gradually lose momentum to the substrate. (ii) *Frictional frustration*: it is typically impossible to maintain nonsliding contacts between colliding particles and the substrate (once the particles are in contact). As the contact force between the particles is typically much greater than that between the particle and substrate, after a collision, the particles will slip on the substrate, losing a large fraction of their momentum due to the presence of kinetic friction.

where m is the mass of the particle, e is the coefficient of normal restitution (~ 1), v is the incoming particle speed, μ is the coefficient of friction between the particle and substrate, and g is the acceleration due to gravity. Assuming comparable friction coefficients between particles and particles and the substrate, the slipping criterion becomes $F_{p\text{-}p} > F_{p\text{-}s}$ which implies that slipping is likely to occur for collision velocities exceeding $v = \mu g \tau_{con}/(1+e)$. Hence, by this argument, slipping seems likely to occur for steel spheres for velocities greater than about $v \simeq (0.5 \times 10^{-2}\ \mathrm{cm/s})/2 \simeq 2.5 \times 10^{-3}$ cm/s. This is a very low value for most recent experiments, for which typical velocities may be of the order of tens of cm/s. For non-head-on collisions, the substrate forces may be more important than estimated above. However, glancing collisions in general will lead to smaller momentum changes and, thus, shorter slipping times. Hence, the effect of ignoring the substrate during glancing collisions may also be relatively slight. We expect that until the later stages of cooling, immediately after a collision, the instantaneous states of the particles are determined by the stronger force at the interparticle contact, with the weaker particle-substrate forces playing minimal roles during the collision.

Following a collision, the particles will slip for an interval of time (determined by the dynamical variables immediately after the collision), after which they will resume a pure rolling state [28]. For typical experimental conditions, significant energy can be lost, since the coefficient of kinetic friction is about 2 orders of magnitude greater than μ_r—i.e., $\mu_k \sim 10^{-1}$ [2,23].

Experimental verification of this picture comes from studies by Painter and Behringer [2] who considered collisions including non-head-on collisions between two identical spherical particles which are both confined to moving on a substrate. Specifically, for a single binary collision, about 63% of the incoming energy of the colliding particles was lost: 6% of the total energy loss was due to collisions and the remaining 57% was due to kinetic friction with the substrate (for steel spheres on aluminum). We would also like to bring to the reader's attention earlier work studying collisions between two small spheres or between a sphere and a flat surface [17] where the impacts were characterized via a three-parameter collisional model.

It is interesting to note that for the case where collisions are frequent enough that the particles are always sliding, the rate of energy loss per particle due to sliding is $(dE/dt)_s = \mu m g v$ and the average rate of energy loss due to collisions is $(dE/dt)_c = [me(2-e)v^2]/\tau_{col}$ (τ_{col} is the time between collisions). The expression for $(dE/dt)_c$ uses the fact that $\Delta E = \frac{1}{2}mv^2 - \frac{1}{2}mv^2(1-e)^2$ is lost per collision. Hence the ratio of the rate of energy loss from sliding to that from collisions is given by

$$\frac{\left(\frac{dE}{dt}\right)_s}{\left(\frac{dE}{dt}\right)_c} = \frac{2\mu g l}{e(2-e)v^2},$$

where l is the mean free path of the particle and $\tau_{col} = l/v$. This implies that one might expect sliding to dominate energy loss at moderately high values of mean free path l and at low incoming speed v, as long as slipping occurs as the result of collisions. Thus, even for small l—say, $l \sim 0.1$ mm—there ought to be, by the argument outlined above for when sliding might occur, a fair range of cooling velocities of a few cm/s and less where sliding occurs and where sliding energy losses outweigh collisional losses.

The object of this work is to study the effects of substrate interactions on a collection of particles, bounded by rigid inelastic walls—that is, cooling to a rest state. We start with all the particles in a *thermalized* state with a 2D Maxwell-Boltzmann (MB) velocity distribution and study how the system evolves under collisional and frictional losses. We are particularly interested in relations between system sizes and collective energy-momentum dissipation mechanisms and their evolution under the influence of collisional and frictional losses. We also examine the evolution of the velocity distributions in these systems, starting from the original 2D MB velocity distribution, as the system suffers energy and momentum losses.

In this paper we introduce a numerical model which incorporates dissipative restitutional interactions between individual granular particles through velocity-dependent coefficients of restitution [19,22,24,30] and the effects of rolling and kinetic frictional forces and torques which the substrate exerts on the particles [21,23,28]. We assume the coefficients of friction to be constant. Throughout this work we use $\mu_r = 0.0025$ and $\mu_s = 0.232$. These correspond to the values measured by Painter and Behringer [3] for 2.38-mm-diam

steel balls moving on a static aluminum substrate. For convenience, we have assumed 5-mm-diam steel balls for this work. Our model also allows for dissipative particle-wall collisions by assuming that the walls are of infinite mass, infinitely hard particles with constant coefficients of normal, and tangential restitution identical to those for interparticle collisions. Following an earlier discussion, our numerical model attempts to capture the essential dynamics relevant to a multiparticle system, confined to a static flat substrate, by considering translational and rotational degrees of freedom which lie in the plane of the motion. Our motivation to neglect the degrees of freedom perpendicular to the substrate is as follows: friction from the spin around the vertical axis is rather slowly damped, presumably due to the fact that the moment arm from the frictional torque is very small. Therefore, there will be a fractionally small energy loss due to this mode. For instance, a sphere (or a top) can spin for long times about a vertical axis, whereas any translational motion will have decayed. This reasoning might overlook the fact that spinning changes the effective friction coefficient for the translational motion. However, we are able to obtain relatively good agreement with the experiments of Painter, suggesting that this is not important.

We have obtained a benchmark of the physical accuracy of our numerical model by incorporating it into a numerical simulation of a granular collider (Painter *et al.* [4]) in Ref. [40], to be published separately. Our numerical results agree well with the experimental ones, which indicates that our numerical model is to some degree physically accurate. We have also explored a larger parameter space than in the experiments by obtaining results for various numbers of particles, input energy, and coefficients of friction.

The rest of this work is structured as follows: Section II gives an overview of the numerical model we used and some details of the initial conditions. Section III gives the results on spatial distributions, particle flow and granular temperature, energy and momentum dissipation, and speed distributions for a bound quasi-two-dimensional system. Section IV gives conclusions and some additional discussion. In the Appendix we present details of the collision rule. We also contrast the average energy loss in a particle-wall collision to a particle-particle collision.

II. NUMERICAL MODEL

The system consists of monodisperse perfectly spherical particles (diameter 5 mm) with two translational degrees of freedom (along the x and y directions) confined to the surface of a square container of dimension 0.25 m (enclosed by walls whose height is much larger than the particle diameter). The particles are allowed to have linear and angular velocities—i.e., $\vec{v}$ and $\vec{\omega}$, respectively—in the plane of the substrate (we neglect vertical spin). As we include the effects of substrate friction and collisional dynamics, our numerical model must take into account the phenomena of *frictional frustration*. The surface exerts frictional forces and torques on the particles—i.e., $\vec{F}_i$ and $\vec{T}_i$, respectively (where $i=r,k$; r for rolling friction and k for kinetic friction [21,23,28]). The static frictional force $\vec{F}_{stat} \leqslant \mu_{stat}\vec{F}_N$ (Coulomb friction criterion for static friction), where μ_{stat} is the coefficient of static friction and $\vec{F}_N$ is the normal force that the substrate exerts on the particle (assuming a point contact between the particle and the substrate), provides the torque to keep a particle (in the pure rolling state) rolling. If $\vec{F}_{stat}$ is less than its maximum allowed value and if the velocity of the instantaneous point of contact between the particle and substrate (slipping velocity) is zero, the particle is in the pure rolling state and the substrate exerts rolling frictional forces and torques so as to oppose the angular motion of the particle. However, if the slipping velocity of the instantaneous contact point is nonzero, the substrate exerts kinetic frictional forces and torques to reduce the slipping velocity to zero, allowing the particle to return to the pure rolling state [23]. Typically, particles slip following a collision for an interval of time [21], after which they return to the pure rolling state. See, e.g., Ref. [13], which details the particle-substrate interactions and its effects on the particle dynamics.

We use an event-driven molecular dynamics technique [39] with the addition of substrate friction to carry out the numerical simulations. This model is implemented by the following steps: (1) we solve the kinematic equations of the particles to determine the shortest time between two successive events (an event is either a collision between two particles or between a particle and a wall), (2) we update the particle dynamical variables by the calculated time, and (3) we use standard kinematic collision rules to calculate the new linear and angular velocities of the colliding particles—i.e., $\vec{v}'$ and $\vec{\omega}'$, respectively (see Ref. [20]). This process continues until the normalized average total kinetic energy per particle has dropped to a value below 10^{-10} of its starting value. Since there is always at least rolling friction, the system should always come to rest in finite time. The particle acceleration is adjusted for changes in the frictional state of the particle during the course of its trajectory (e.g., a slipping particle resumes rolling). We make the assumption that the particles are hard spheres with zero contact time (in reality, the contact time for steel spheres is $\sim 10^{-5}$ s [3]). The restitutional loss is modeled via the use of velocity-dependent coefficients of restitution [19,22,24,30], as detailed in the Appendix.

A key point of the model is that we assume that the collisional force integrated over the collision time is much stronger than the frictional force with the substrate over the same time. Therefore, the post-collision properties of a pair of particles are specified entirely by the incoming properties of the particles via a collision rule, thus allowing a substantial reduction in computational cost and complexity. This means that in a typical case, the particles will be slipping on the substrate immediately after the collision. This assumption appears to be reasonable until the later times of the cooling process, at which point much of any initial energy will have been dissipated.

To generate initial conditions we carry out the following procedure. All the particles in the system are first placed on a lattice and are assigned random linear velocities $\vec{v}_i$. At this time, all interactions with the substrate are turned off, collisions between particles are elastic, and each $\vec{\omega}_i$ is set to zero. Before the simulation commences, any residual flow is re-

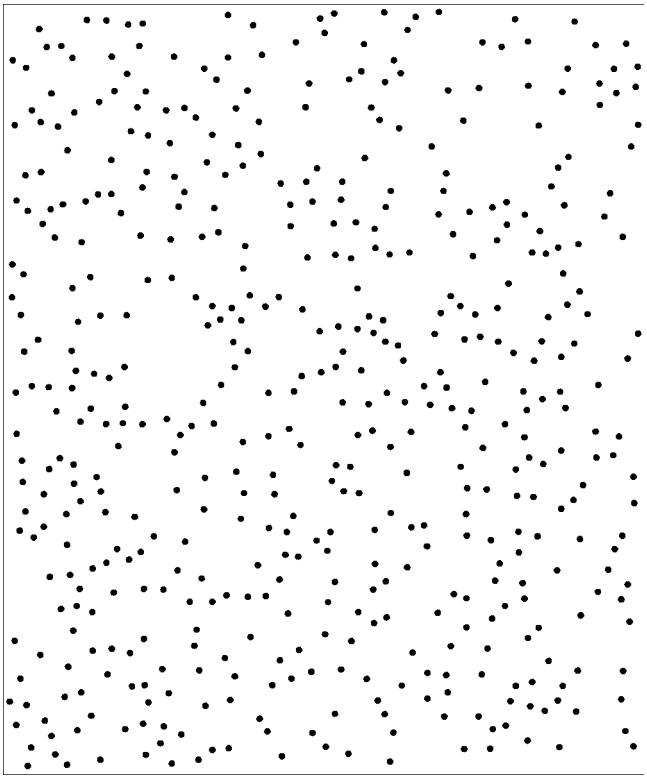

FIG. 2. Particle positions at time $t=0$ s, after thermalization, before the simulation begins.

moved by calculating the initial momentum per particles ($\vec{p}$) and subtracting $\vec{p}$ from the momentum of each particle. The particles are allowed to thermalize by suffering elastic collisions among themselves and with the walls for $\sim$1000 collisions per particle. This is done to allow the particles to have a 2D MB velocity distribution at the end of the thermalization process. A perfectly elastic binary collision rule is used in the thermalization process. After the thermalization process, the angular velocities of the particles are calculated from the respective linear velocities, assuming all the particles to be in the pure rolling state. At that point, the particle-substrate frictional interaction and restitutional losses are switched on.

III. NUMERICAL RESULTS

We have carried out numerical studies for different system sizes (50–1600 particles). However, here, we will primarily focus on results for a monodisperse 500-particle system; unless otherwise specified, results pertain to this particle number. We have divided our results into four sections: spatial distributions, particle flow patterns and granular temperature, energy and momentum dissipation; and speed distributions.

A. Spatial distributions

Figures 2 and 3 show the particle positions after thermalization (but before the substrate friction is turned on) and after the simulation stops, respectively. At time $t=0$, the particles are randomly distributed throughout the system. But by

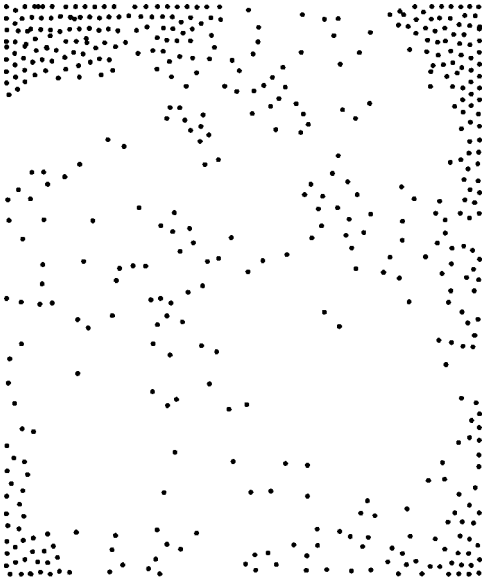

FIG. 3. Particle positions at time $t=8.64$ s, once the simulation stops.

$t=8.64$ s, when the particles have come to rest, they have preferentially accumulated in the vicinity of the corners and the walls with a few particles scattered away from the walls. We have observed this novel phenomenon of accumulation of particles in the vicinity of the walls for all the system sizes that we have studied. Figure 4, which is a plot of the final spatial configuration of a 1600-particle system after all the particles have come to rest (2.79 s), is an example for a large system.

To quantify the overall drift of particles towards the walls, we calculated $d_{average}$, the average distance of a particle from the closest wall, as a function of time. In Fig. 5(a), we show the time evolution of this quantity normalized by the value $L/6$, the value that would occur for a uniform placement of

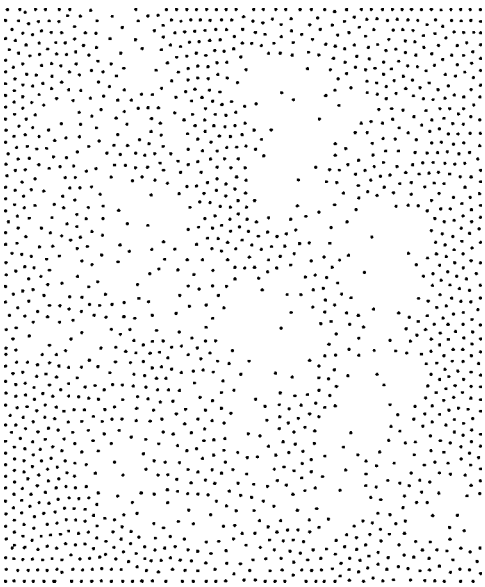

FIG. 4. Particle positions for a 1600-particle system at time $t=2.79$ s, once the simulation stops.

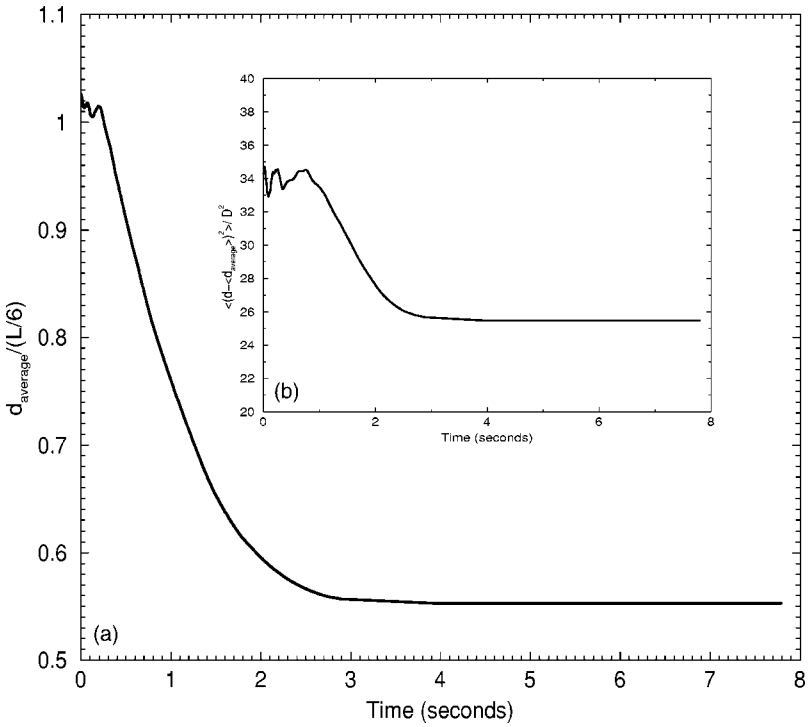

FIG. 5. (a) $d_{average}/(L/6)$ as a function of time in seconds. The factor $L/6$ is the value of $d_{average}$ for a uniform placement of particles. (b) $\langle (d-\langle d_{average}\rangle)^2\rangle / D^2$ as a function of time where D is the particle diameter.

particles. We observe $6d_{average}/L$ to oscillate initially (due to random collisions between energetic particles), after which it decreases steadily (due to a net flow of particles towards the walls) and approaches a plateau well below 1. By considering the fluctuations about the average distance of a particle from the closest wall, we gain insight into the compactness of the bands near the walls. In Fig. 5(b) we have plotted the mean-square fluctuation about $d_{average}$ normalized by a particle diameter as a function of time. From these two measures, we see that the particles do not have a distinct direction of flow until $t \sim 1$ s. However, after that time, the particles drift steadily towards the walls (as the variance of $d_{average}$ and $d_{average}$ decrease with increasing time). As particles in the system begin losing their energy and momentum, the time between successive collisions gets longer, hence the plateau from 2.5 s onward.

B. Particle flow and granular temperature

Figure 6 combines spatial configurations and velocity vector field plots on the left and right columns, respectively, at different times—namely, 0 s (top), 1.18 s (center), and 2.56 s (bottom). For each velocity vector diagram, the length of the longest arrow represents the magnitude of largest local velocity at that instant and the length of the other arrows scale accordingly. Immediately after thermalization, the particles are homogeneously distributed throughout the system without any preferred direction of flow. This trend persists at early times (shortly before $t \simeq 0.60$ s), after which a tendency for the particles to flow towards the walls becomes apparent. This trend continues, Fig. 6, center, as particles form clusters near the walls.

Further insight into the system behavior can be obtained by following the time evolution of the variance of the velocity T_g and by making comparisons to the time evolution of the global velocity variance. To carry out the analysis, we have set a threshold distance d_{thres} which is used to distinguish between particles lying in the vicinity of the walls (provided their shortest distance from the walls is less than or equal to d_{thres}) and those particles whose shortest distance from the walls exceeds d_{thres}. We have calculated the velocity variance for the two groups of particles by using the relation

$$T_g = \langle \vec{v} - \langle \vec{v} \rangle \rangle^2,$$

where here $\vec{v}$ is the velocity of each particle in one of the groups and $\langle \vec{v} \rangle$ is the average velocity of the particles in that group.

Figure 7 shows the time of evolution of the velocity variance of all the particles collectively and those in the vicinity and away from the walls. We have set $d_{thres} = 3d$ where d is the particle diameter. We find that the velocity variance of the particles in the vicinity of the walls fluctuates significantly at earlier times ($\sim 0.05-0.06$ s) as there are relatively few particles in this group. As the flow of the particles towards the walls becomes predominant (decreasing value of $d_{average}$) the fluctuations about the average velocity of the particles close to the walls fall below that of the other particles. The average velocity of these particles will be very close to zero as these particles are moving in opposite directions (towards the four walls). The velocity variance for the particles in the vicinity of walls is slightly lower than for those away from the walls, which reflects the higher-energy losses one might expect for a region of locally higher density.

C. Energy and momentum dissipation

The time evolution of the number of particles in the slipping state, n_{slip}, the number of particles in the pure rolling

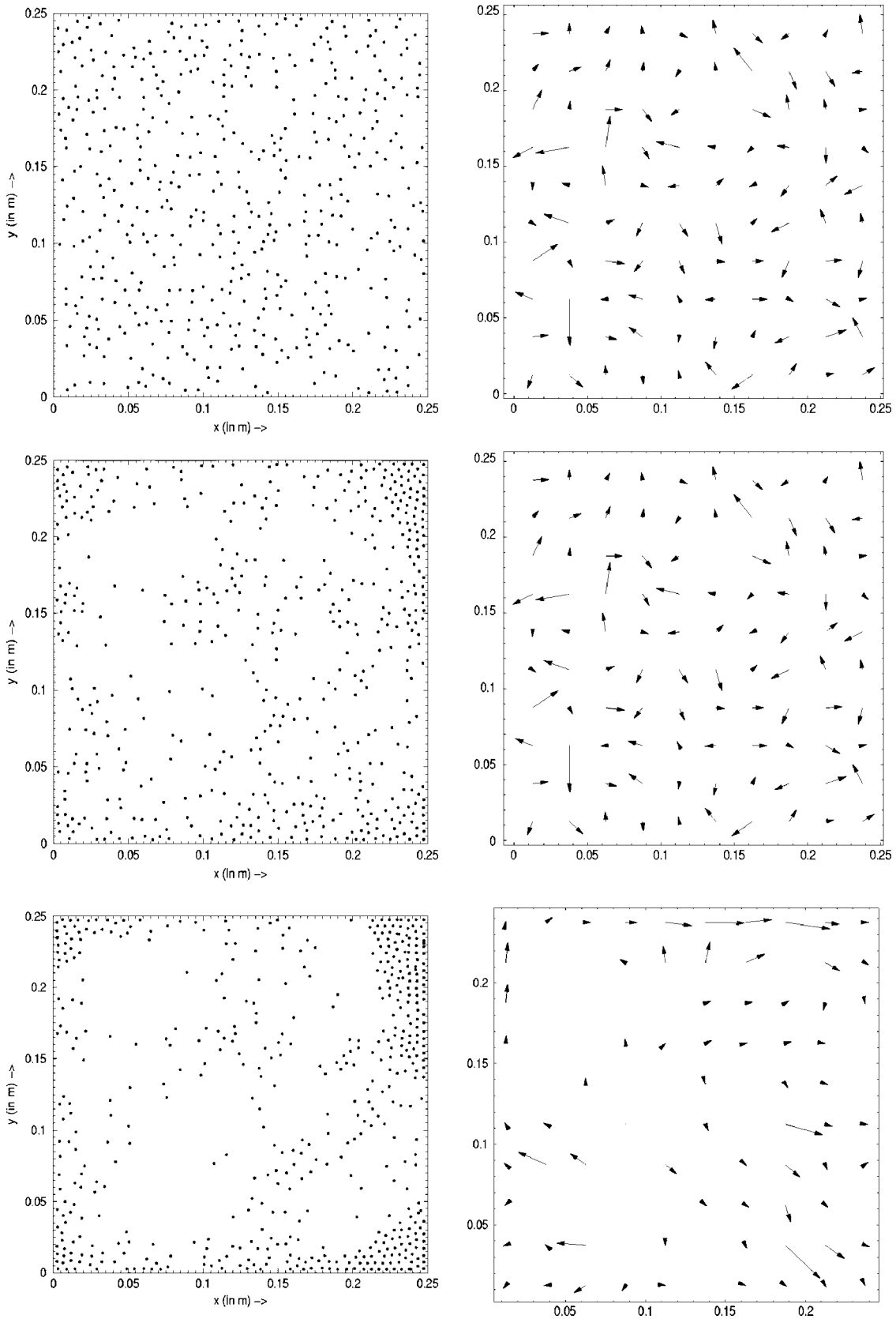

FIG. 6. Particle positions (left column) and velocity vector field (right column) for times immediately after thermalization 0 s (top), 1.18 s (center), and 2.56 s (bottom). In each of the velocity diagrams, the arrow of the longest length represents a maximum average speed for that frame. These values are, respectively, 0.99, 0.082, and 0.02 (in m/s) for 0 s, 1.18 s, and 2.56 s. For all the figure boxes, the *x* and *y* axes range from 0 to 0.25 m.

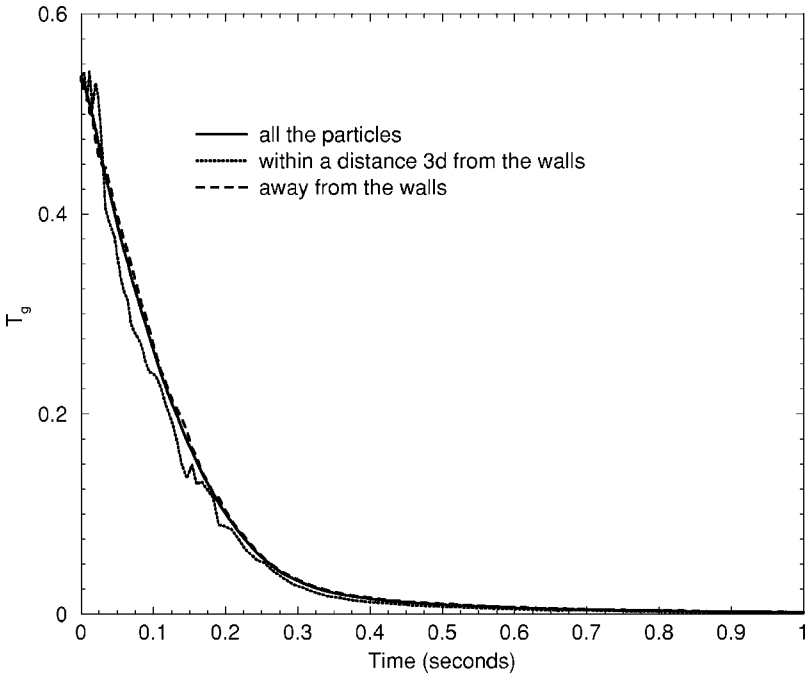

FIG. 7. Granular temperature T_g (approximate) as a function of time for three groups of particles: all the particles in the system (N), those lying at a distance $3d$ (d=particle diameter) from the walls (N_{3d}), and particles lying away from the vicinity of the walls ($N-N_{3d}$).

state, n_{roll}, and the number of particles moving, n_{move}, provides a useful picture of the dynamics. Figure 8 demonstrates key features for the 500-particle system. Up to about $\sim 10^{-3}$ s, almost all particles are rolling. Near $\sim 10^{-1}$ s, the number of rolling particles has reached a minimum or, alternatively, almost all moving particles are sliding. In the later stages, almost all particles that are moving are rolling, and the pure rolling state dominates until all the particles come to rest. We can understand this transition back to the rolling state by noting that for sliding friction, the acceleration is constant; thus, the distance required to stop sliding, $d_{stop} \propto v^2$. Consequently, as the system cools, the time and distance spent sliding after a collision decrease relatively rapidly.

It is also interesting to give an approximate idea of the region in the system where most of the particles are slipping or rolling relative to the distance to the closest wall. Figure 9 plots $d_{average}$ (normalized by $L/6$) for all the moving particles (n_{move}) n_{roll} and n_{slip} as a function of time. On average, those particles that are slipping are the closest to the walls.

The value of $d_{average}$ is sensitive to fluctuations if the number of particles used to compute it is small. At $t \sim 0$, the

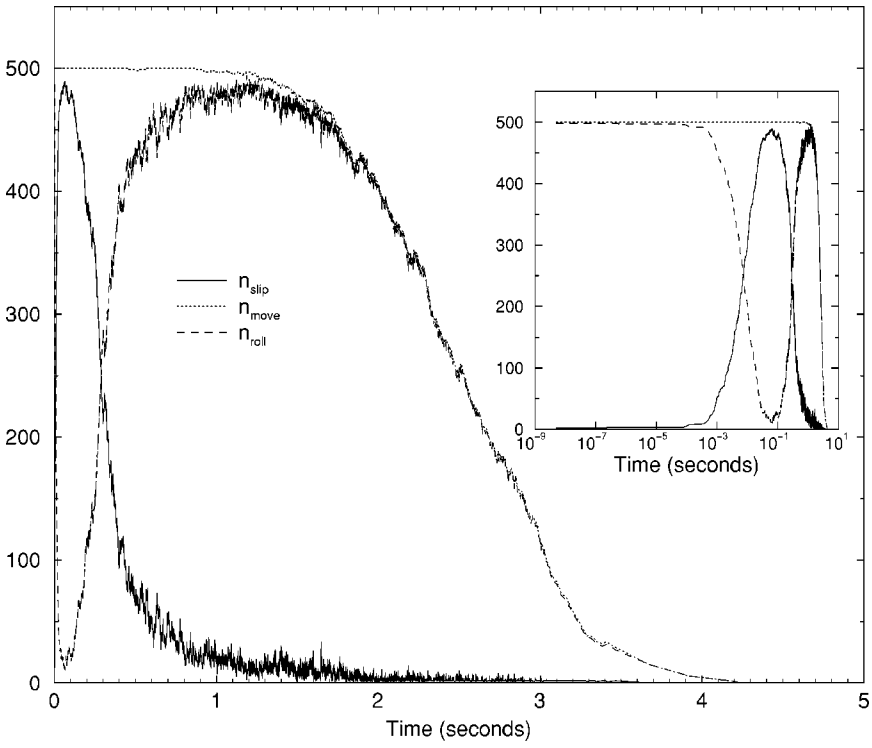

FIG. 8. Total number of particles that are slipping, moving, and rolling as a function of time. The inset shows the same data on a linear-logarithmic scale to focus on the earlier times.

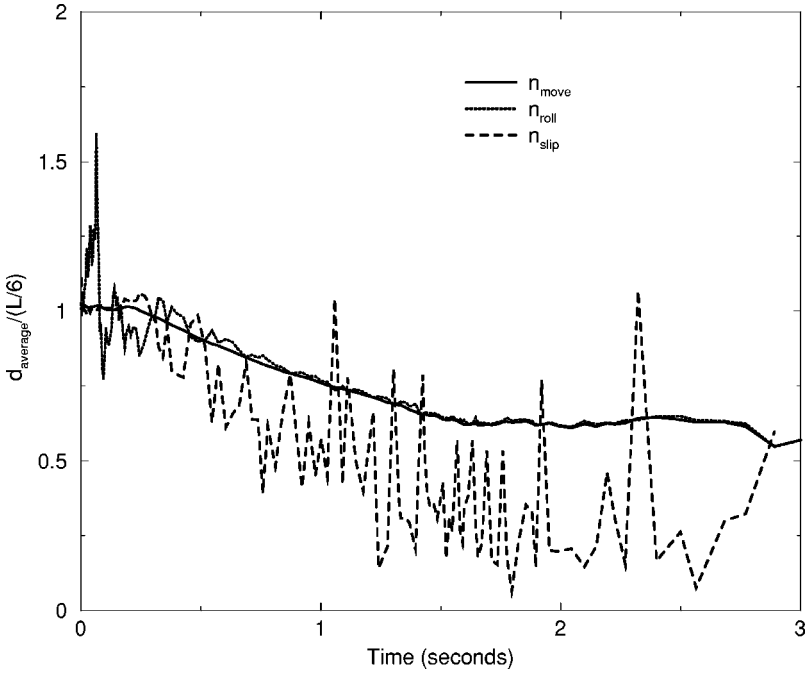

FIG. 9. $6d_{average}/L$ of n_{move}, n_{slip}, and n_{roll} as a function of time.

fluctuations in the values of $d_{average}$ for n_{roll} (n_{slip}) are small (large) as most of the particles are in the pure rolling state. However, for times approaching ~ 0.3 s, with increasing number of particles in the slipping state, the fluctuations in the values of $d_{average}$ for n_{roll} (n_{slip}) become high (low). For times $t \geqslant 0.3$ s, with increasing number of particles in the pure rolling state, the value of $d_{average}$ for n_{slip} fluctuates significantly every time a particle pair collides. These fluctuations are superimposed on a monotonic decrease of $d_{average}$ for all particle states and for n_{slip} in particular. Hence, $d_{average}$ vs t for n_{slip} indicates that initially most of the collisions are uniformly distributed on the surface, but that as time evolves, the collisions occur at decreasing distances from the walls. In fact, for times $0.05\ \text{s} \leqslant t \leqslant 0.3$ s, as most of the particles are in the slipping state, the value of $d_{average}$ for n_{slip} closely follows the value for n_{move}. Later, $d_{average}$ for n_{roll} approaches n_{move} as the majority of the particles are in the pure rolling state.

The time evolution of the normalized average total kinetic energy, along with its components (translational and rotational), provides further insight into the average dynamical state of the particles. The average energies, Fig. 10, have been normalized by their values immediately after thermalization, where all particles are rolling without slipping. Since the velocities satisfy a Maxwell-Boltzmann distribution at that time, necessarily so do the spins. The various curves for

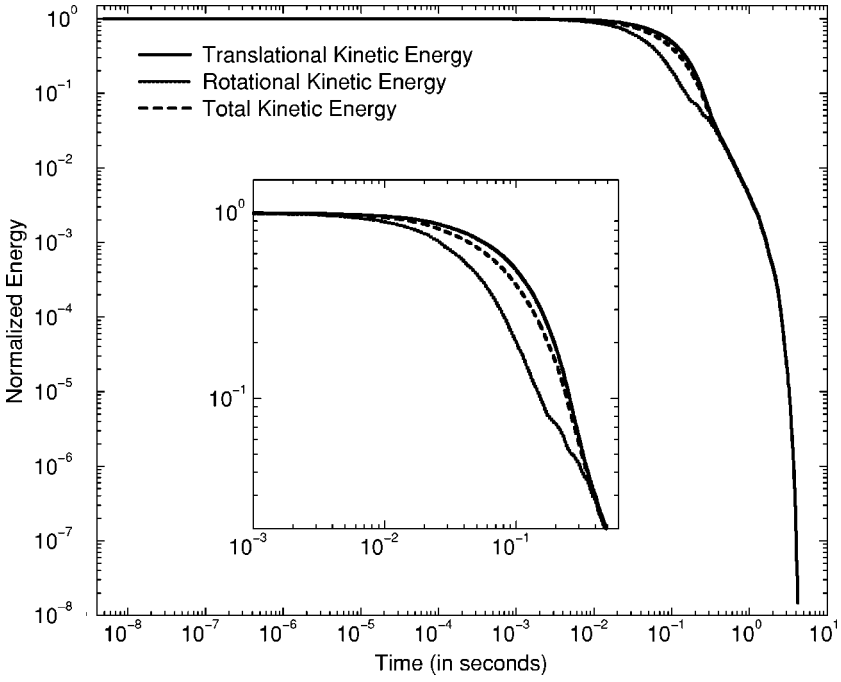

FIG. 10. Normalized translational, rotational, and total kinetic energies of the system as a function of time. The inset shows in detail the normalized energy profile when $n_{slip} > n_{roll}$.

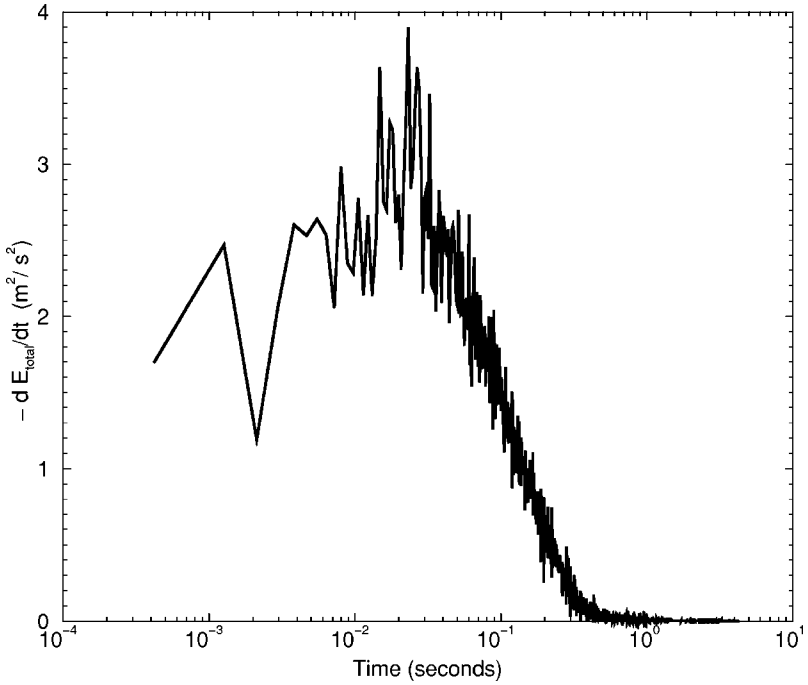

FIG. 11. Rate of decrease of average total kinetic energy (m^2/s^s) vs time.

different energies versus time coincide with each other at all times except for the time interval $0 \lesssim t \lesssim 0.29$ s when the dynamics of the particles is dominated by the slipping state ($n_{slip} > n_{roll}$). The disparity in the normalized energy curves becomes most noticeable at $t \simeq 0.06$ s when n_{slip} is maximum. We emphasize that in the region where the three curves are separate, this separation is indicative of the fact that the slipping particles have less rotational energy on average than they would have if they were rolling without slipping.

We also consider in Fig. 11 the rate of decrease of total kinetic energy as a function of time to see if there was a particular dynamical state in which the energy loss was maximum. Not surprisingly, the time at which the maximum value of the rate of loss of average total kinetic energy coincides with that at which the maximum of n_{slip} occurs.

A key point is that clustering near the walls is associated with the presence of substrate friction. When all substrate frictional forces (and torques) are removed allowing dissipation through solely particle-particle and particle-wall collisions, clustering near the walls does not occur, at least for the parameter ranges considered here. To show this, a simulation was carried out neglecting substrate effects and allowing only collisional dissipation (using the same initial conditions as for the simulation with substrate friction). Figure 12 shows final particle positions when the average normalized kinetic energy of the particles has fallen below 10^{-10}. In this simulation, as elsewhere, we used velocity-dependent coefficients of restitution so that as $v_n \to 0$ the collisions became increasingly elastic. Hence, as velocities drop to 0, collapse is not expected to occur (in the absence of surface friction). We have plotted the time evolution of $d_{average}$ and the fluctuation about $d_{average}$ in Figs. 13(a) and 13(b), respectively. The highly elastic collisions between the particles (relative to the case with friction) result in the near invariance of $d_{average}$ and very low fluctuations about it with time. The system is seen to behave like a pseudokinetic gas bound by four walls. By contrast, with constant coefficients of restitution (the interparticle coefficients of restitution, defined in the Appendix, were taken to be $\alpha_p = 0.9$ and $\beta_p = -0.85$) both for interparticle and particle-wall collisions, the particles show a tendency to flow towards the corners and the walls, Figs. 14 and 15, with elastic and inelastic walls, respectively.

An important question is, why do the particles concentrate at the corners and edges of the walls? In the Appendix we show that, on average, a particle loses a greater fraction of its energy during slipping after suffering a collision with a wall than it does after colliding with another identical particle. For the two cases, we first calculate the total energy of the particle after collision, E_o; we then calculate the total energy

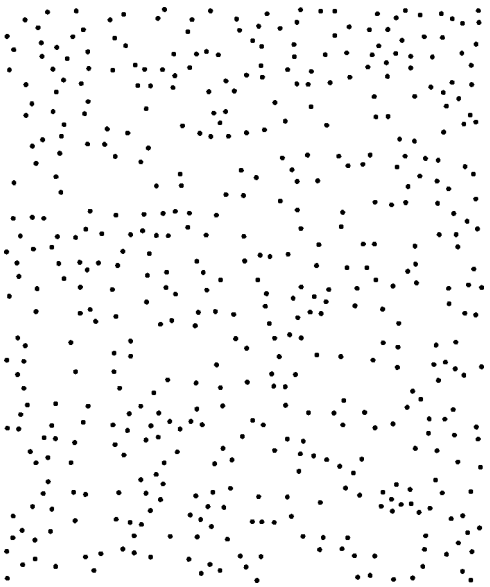

FIG. 12. Final particle positions when substrate friction has been removed.

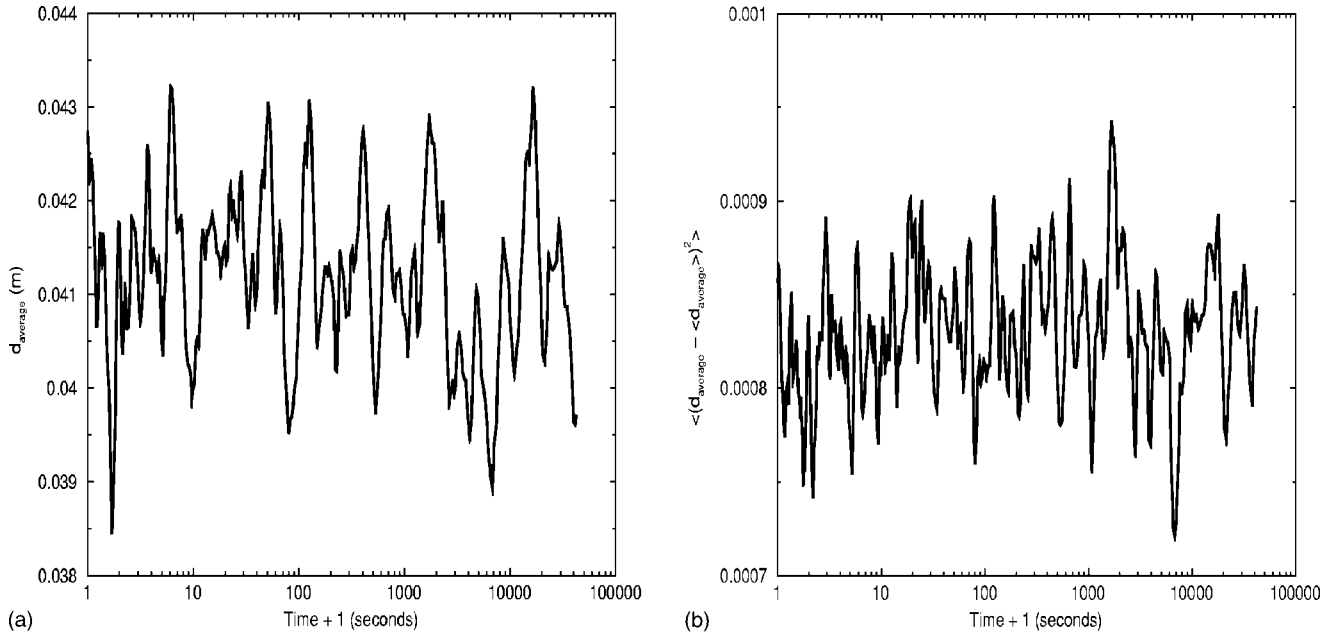

FIG. 13. (a) Variation of $6d_{average}/L$ with time and (b) variation of variance (with respect to $\bar{\bar{d}}$) with time. These are results from the simulations carried out using velocity-dependent coefficients of restitution.

of the particle after it has stopped slipping, E_f. Due to geometrical considerations, the probability of interparticle glancing collisions is much higher than for particle-particle impacts. As a result, the momentum change per particle, the relative slipping velocity per particle, and the slipping times are much smaller after an interparticle impact as opposed to a particle-wall impact. Tables I and II show the energy losses for some special cases of interparticle and particle-wall collisions. The increased energy dissipation for particle-wall versus particle-particle collisions leads to clustering in a way that bears some parallels to the conventional clustering instability [27]: near-wall regions preferentially cool, resulting in a locally lower pressure, which in turn leads to an influx of particles.

As a further exploration of wall effects, we removed the inelastic walls by introducing 2D periodic boundary conditions, kept all other aspects of our substrate frictional simulation unchanged, and carried out simulations for a range of particle numbers. Figures 16 and 17 show initial and final particle configurations for a 1600-particle system. Clustering is observed to occur as the system cools (with all the particles coming to rest) and becomes pronounced with increas-

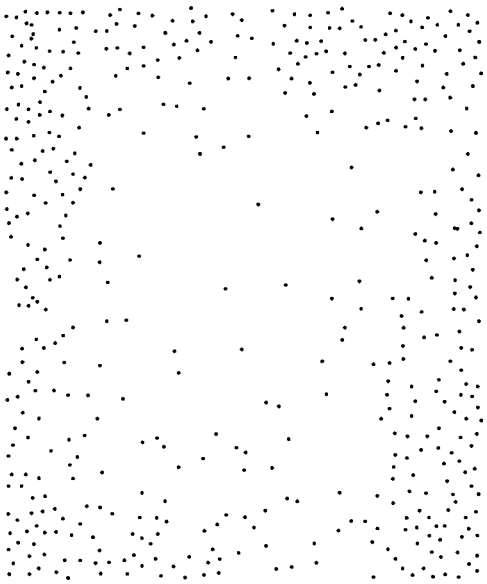

FIG. 14. Final particle positions for a 500-particle system with $\alpha_p = 0.9$ and $\beta_p = -0.85$ and elastic walls (particle-substrate friction is absent).

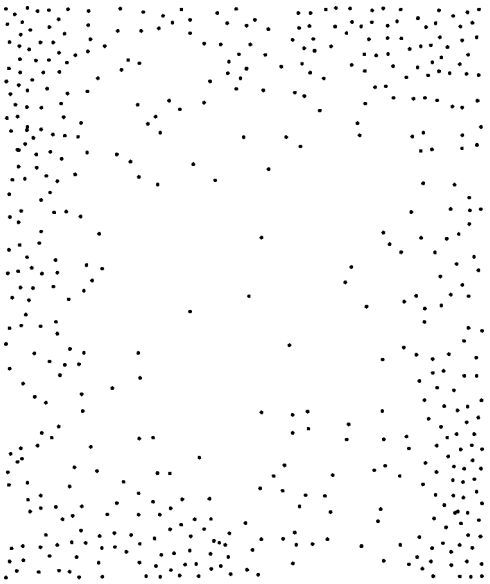

FIG. 15. Final particle positions for a 500-particle system with $\alpha_p = 0.9$ and $\beta_p = -0.85$ and inelastic walls—i.e., $\alpha_w = 0.9$, $\beta_w = -0.85$ (particle-substrate friction is absent).

TABLE I. Comparison of the average energy loss for interparticle collisions for different special cases. The special case of the normal impact means that the tangential component of the linear velocity and the normal component of the angular velocity (assuming that the colliding particles are in the pure rolling state), before collision, are zero. In the case of $|[(d/2)(\vec{\omega}_i+\vec{\omega}_j)\cdot\hat{n}]|=|[(d/2)(\vec{\omega}_i+\vec{\omega}_j)\cdot\hat{t}]|$, the normal and tangential components of the sum of the angular velocities of the colliding particles are assumed to be equal for ease of calculation. The last two entries were obtained by carrying out simulations for a 200-particle system using fixed coefficients of restitution.

Case	α	β	$\langle \Delta E/E_k^f \rangle_{ppc}$
Normal impact	0	0	0.271
Normal impact	1	−1	0.326
Normal impact	1	1	0.680
$\lvert(d/2(\vec{\omega}_i+\vec{\omega}_j)\cdot\hat{n})\rvert=\lvert(d/2(\vec{\omega}_i+\vec{\omega}_j)\cdot\hat{t})\rvert$	0	0	0.288
$\lvert(d/2(\vec{\omega}_i+\vec{\omega}_j)\cdot\hat{n})\rvert=\lvert(d/2(\vec{\omega}_i+\vec{\omega}_j)\cdot\hat{t})\rvert$	1	−1	0.270
$\lvert(d/2(\vec{\omega}_i+\vec{\omega}_j)\cdot\hat{n})\rvert=\lvert(d/2(\vec{\omega}_i+\vec{\omega}_j)\cdot\hat{t})\rvert$	1	1	0.469
200-particle simulation	0	1	0.050
200-particle simulation	1	−1	0.231

ing number of particles. The absence of walls does not substantially change the behavior of the system in terms of variation of its average kinetic energy or number of particles slipping, rolling, or moving with time (Fig. 18).

D. Speed distributions

Various studies [4,14,15] have shown that for inelastic particles, the velocity distributions deviate from a 2D MB distribution. In our case, dissipative interactions are enhanced by interactions with the substrate, and we might expect strong deviations from a Maxwell-Boltzmann distribution as time evolves. We investigated the evolution of the speed distribution, starting from MB, for various system sizes and found that the qualitative evolution of the distribution is insensitive to particle number. Thus, we only discuss

TABLE II. Comparison of the average energy loss for particle-wall collisions for different special cases. The special case of the normal impact means that the tangential component of the linear velocity and the normal component of the angular velocity (assuming that the particle is in the pure rolling state), before collision, are zero. The general case is when the normal and tangential components of the linear and angular velocities, before collision, are nonzero.

Case	α	β	$\langle \Delta E/E_k^f \rangle_{pwc}$
Normal impact	0	0	0.714
Normal impact	1	−1	0.816
Normal impact	1	1	0.087
General case	0	0	0.135
General case	1	−1	0.408
General case	1	1	0.118

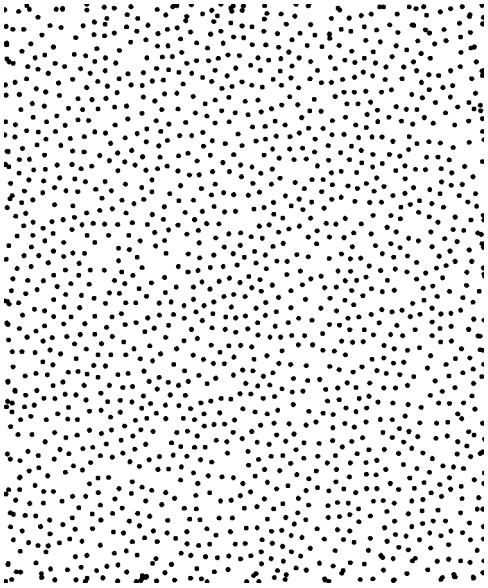

FIG. 16. Particle positions of a 1600-particle system (without any walls) at 0 s.

results for the 500-particle system. The fluctuation speed v is defined to be $v=|\vec{v}-\vec{v}_{\text{c.m.}}|$ where $\vec{v}_{\text{c.m.}}$ is the global center-of-mass velocity (which is nearly zero). Note that as there is some net flow to the walls, the fluctuation speed distribution may be influenced by using the global center of mass velocity. For early times, $t\lesssim 0.06$ s, the distribution is well described as MB [see Fig. 19(a)]. For intermediate times—say, $t\gtrsim 0.07$ s—the velocity distribution evolves to $P(v)\sim A_3 v\ \exp\{[-A_0(v-A_1)^2]\}$ and finally at relatively long times to $P(v)\sim A_0 v e^{(-A_3 v)}$ or, possibly, $P(v)\sim A_0 v^{\alpha}$. However, at the very latest times $t\gtrsim 2.2$ s the statistics are not sufficient to distinguish between an exponential decay or a power law [Fig. 19(b)]. Note that during the last stages of the simulation—say, 2.27 s$\lesssim t\lesssim$2.77 s—a significant number of

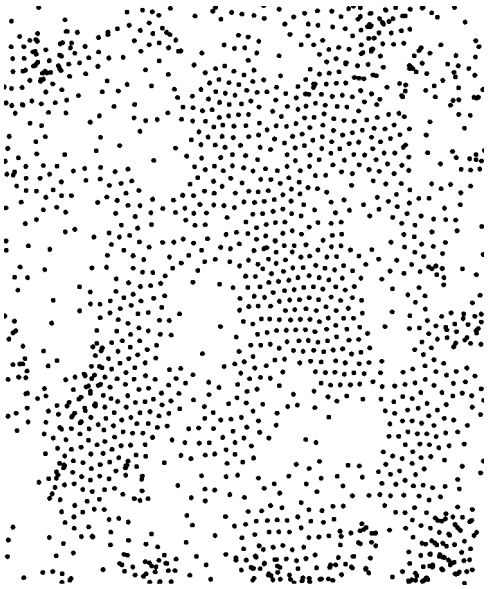

FIG. 17. Particle positions of a 1600-particle system (without any walls) when all the particles have come to rest at 3.49 s.

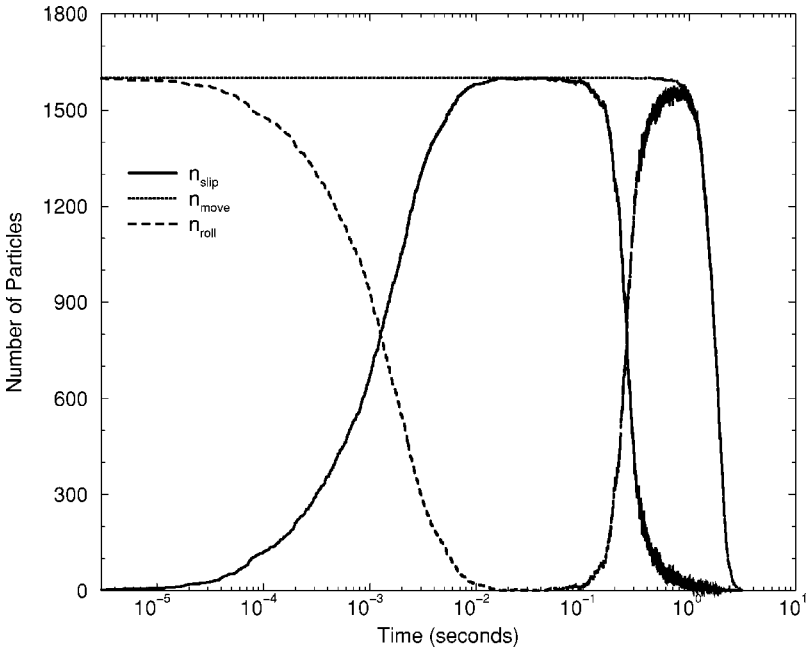

FIG. 18. Number of particles slipping, moving, and rolling with time for a 1600-particle system (without walls).

the particles in the system are at rest (Fig. 8). This evolution of the functional form of the distribution of fluctuation speeds is very similar to the experimental results of Ref. [4], where the authors observed a transition from a MB distribution to an exponential distribution at long times.

IV. CONCLUSION

The numerical model presented in this paper addresses the issue of surface friction and particle collisions in the presence of a substrate by accounting for frictional forces and torques between the particles and substrate. The key assumption of the model is that if particles collide, the velocity and spin states immediately after the collision are determined solely by collision rules involving the incoming states of the particles. That is, the effect of friction with the substrate was assumed to be unimportant during the very short time of the collision. This typically leads to a slipping of the particles on the substrate after a collision. We use this numerical model to compute the evolving dynamics of a quasi-two-dimensional many-body system enclosed by inelastic walls. Particle collisions with the inelastic walls are more effective at removing energy than are particle-particle collisions, leading to

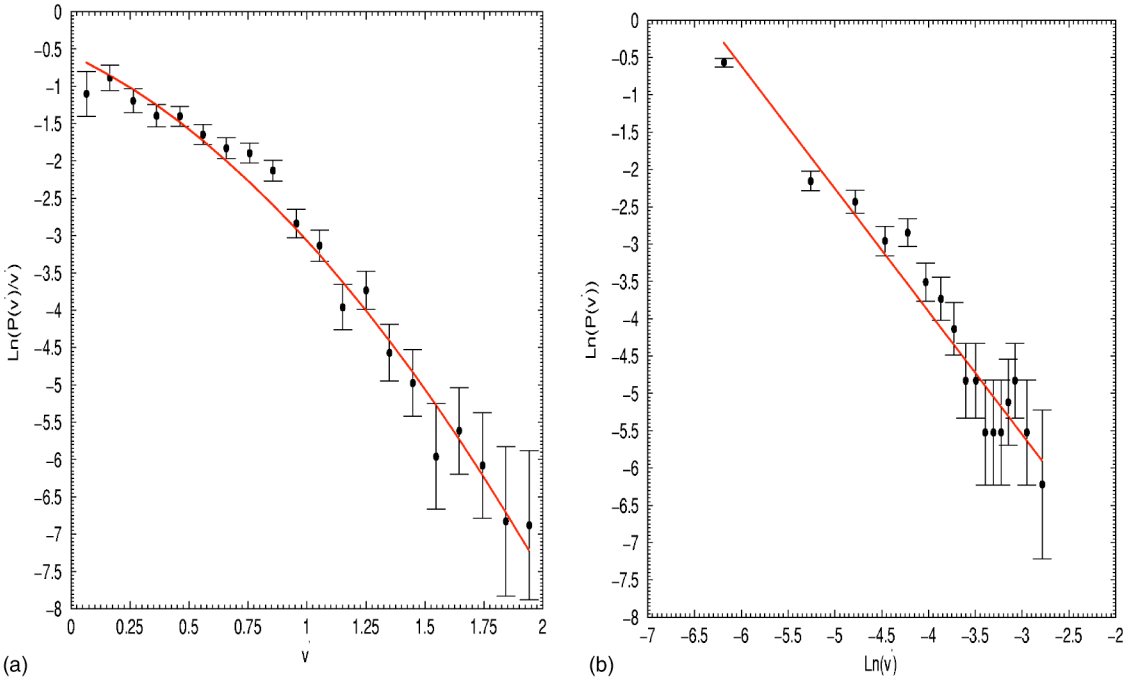

FIG. 19. Velocity distribution fit for times (a) 0 s, $P(v) \sim A_3 v \exp[(-A_0(v-A_1)^2]$, and (b) 2.269 s, $P(v) \sim A_0 v^{\alpha}$.

flow of the particles towards the walls, where they accumulate. This effective collision-induced flow towards the walls is a consequence of dissipation and, in particular, dissipation from surface friction. A greater momentum change results in a longer slipping interval and is thereby more dissipative due to kinetic friction for the particle in question. The dissipation rate of the average total kinetic energy of the particles is greatest when $n_{slip} > n_{roll}$. In the presence of surface friction, the velocity distribution of the particles changes from a MB distribution (when the particles are in the thermalized state) to a distribution, possibly exponential in character, as seen in the experiments [4]. Finally, the results do not vary significantly for the different system sizes that we have considered.

To our knowledge, these simulations are the first to consider simultaneously surface friction and collisional dynamics of large collections of particles and their effects on two-dimensional multiparticle dynamics. We have used constant values for the coefficients of friction to model surface friction in quasi-two-dimensional many-body systems, which has produced results which agree well with experimental ones [40]. The model necessarily has limitations. Specifically, the assumption that the immediately post-collision particles have a state that is independent of the frictional forces from the substrate is not likely to be valid for very slow velocities. However, we expect that this shortcoming of the model becomes relevant only at very late times in the simulation.

ACKNOWLEDGMENTS

This work was supported by NSF Grant Nos. DMR-0137119 and DMS-0204677 and by NASA Grant No. NAG3-2372.

APPENDIX

Collision dynamics rules

In this appendix, we first briefly discuss the collision rule that we use to determine the final states immediately after a collision. We then consider the energy losses for particle-particle and particle-wall collisions.

The two special cases for the binary collision rule for two spherical particles i and j with different masses ($m_i \neq m_j$) of radii a, positions $\vec{r}_i$ and $\vec{r}_j$, linear velocities $\vec{v}_i$ and $\vec{v}_j$, and angular velocities $\vec{\omega}_i$ and $\vec{\omega}_j$, respectively, is given by Eq. (A1). For collisions of two particles i and j with identical masses—i.e., $m_i = m_j$—the collision rule is [24]

$$\vec{v}_i' = \vec{v}_i - \frac{1+\alpha}{2}\vec{v}_n - \frac{q}{2}\frac{1+\beta}{1+q}(\vec{v}_t + \vec{v}_r),$$

$$\vec{v}_j' = \vec{v}_j + \frac{1+\alpha}{2}\vec{v}_n + \frac{q}{2}\frac{1+\beta}{1+q}(\vec{v}_t + \vec{v}_r),$$

$$a\vec{\omega}_i' = a\vec{\omega}_i + \frac{1+\beta}{2(1+q)}\hat{n} \times (\vec{v}_t + \vec{v}_r),$$

$$a\vec{\omega}_j' = a\vec{\omega}_j + \frac{1+\beta}{2(1+q)}\hat{n} \times (\vec{v}_t + \vec{v}_r).$$

For particle-wall collisions (as walls are infinitely massive)—i.e., $m_j \gg m_i$,

$$\vec{v}_i' = \vec{v}_i - (1+\alpha)\vec{v}_n - q\frac{1+\beta}{1+q}(\vec{v}_t + \vec{v}_r),$$

$$\vec{v}_j' = 0,$$

$$a\vec{\omega}_i' = a\vec{\omega}_i + \frac{1+\beta}{1+q}\hat{n} \times (\vec{v}_t + \vec{v}_r),$$

$$a\vec{\omega}_j' = 0,$$

where

$$\vec{v}_c = \vec{v}_i - \vec{v}_j - a(\vec{\omega}_i + \vec{\omega}_j) \times \hat{n},$$

$$\hat{n} = \frac{r_i - r_j}{|r_i - r_j|},$$

$$\vec{v}_c' \cdot \hat{n} = -\alpha \vec{v}_c \cdot \hat{n},$$

$$\vec{v}_c' \times \hat{n} = -\beta \vec{v}_c \times \hat{n},$$

$$\vec{v}_n = \hat{n}(\vec{v}_i - \vec{v}_j) \cdot \hat{n},$$

$$\vec{v}_t = \vec{v}_i - \vec{v}_j - \vec{v}_n,$$

$$\vec{v}_r = -a(\vec{\omega}_i + \vec{\omega}_j) \times \hat{n},$$

$$\vec{v}_c = \vec{v}_n + \vec{v}_t + \vec{v}_r.$$

For particle-wall collisions, the normal unit vector $\hat{n}$ is the unit vector perpendicular to the wall-surface collision pointing from the contact point with the wall to the center of the particle. We attach a coefficient p or w for particle-particle or particle-wall collisions. Further details can be found in Refs. [19,22,24,30].

Average normalized energy loss for particle-particle and particle-wall collisions

The purpose of this calculation is to determine whether, on average, a particle loses more energy due to kinetic friction after a collision with a wall or with another particle, using the evolution rules of the model. For the two cases, we first calculate the change in total kinetic energies E_k of the particle(s) after collision and at the end of slipping. The particle dynamical variables after a collision can be obtained from the collision rule [20].

The unprimed and primed quantities represent dynamical variables before and after collision, respectively. $E_k^{\,i}$ is given by the sum of rotational and translational kinetic energies.

For an interparticle collision $E_k^{\,i}$ is the sum of the kinetic energies of the colliding particles whereas, for a particle-wall impact, $E_k^{\,i}$ is the total kinetic energy of the colliding particle. Hence for interparticle collisions $E_k^{\,ij}$ is

$$E_k^{ij} = \frac{1}{2}m\vec{v}_i' \cdot \vec{v}_i' + \frac{1}{2}I\vec{\omega}_i' \cdot \vec{\omega}_i' + \frac{1}{2}m\vec{v}_j' \cdot \vec{v}_j' + \frac{1}{2}I\vec{\omega}_j' \cdot \vec{\omega}_j', \tag{A1}$$

where $I=\frac{2}{5}ma^2$ is the moment of inertia about a spherical particle diameter of radius a and mass m. For particle-wall impacts,

$$E_k^{i} = \frac{1}{2}m\vec{v}_i' \cdot \vec{v}_i' + \frac{1}{2}I\vec{\omega}_i' \cdot \vec{\omega}_i'. \tag{A2}$$

We make the assumption that the condition of *frictional frustration* is satisfied for the colliding particle(s), hence resulting in a finite slipping velocity $\vec{u}$ of each colliding particle. We calculate the slipping velocity $\vec{u}$ which the particle(s) have after impact and use $\dot{\vec{u}}$ to calculate the duration of slipping t_{slip}, given by

$$t_{slip} \simeq \left| \frac{\vec{u}}{\dot{\vec{u}}} \right|.$$

We use t_{slip} along with the linear and angular decelerations $\vec{a}_k$ and $\vec{\dot{\omega}}$, respectively, to calculate the linear and angular velocities $\vec{v}$ and $\vec{\omega}$, respectively, after the particles have stopped slipping through the following relations:

$$\vec{v}'' = \vec{v}' + \vec{a}_k t_{slip}, \tag{A3}$$

$$\vec{\omega}'' = \vec{\omega}' + \dot{\vec{\omega}} t_{slip}, \tag{A4}$$

where the double prime represents dynamical variables when the particle(s) has just stopped slipping.

We can calculate E_k^{f}, the total kinetic energy of the particle(s) just after slipping stops, by

$$E_k^{f} = \frac{1}{2}m\vec{v}_i'' \cdot \vec{v}_i'' + \frac{1}{2}I\vec{\omega}_i'' \cdot \vec{\omega}_i'' + \frac{1}{2}m\vec{v}_j'' \cdot \vec{v}_j'' + \frac{1}{2}I\vec{\omega}_j'' \cdot \vec{\omega}_j'' \tag{A5}$$

for interparticle impacts and by

$$E_k^{f} = \frac{1}{2}m\vec{v}_i'' \cdot \vec{v}_i'' + \frac{1}{2}I\vec{\omega}_i' \cdot \vec{\omega}_i'' \tag{A6}$$

for particle-wall impacts.

The change in total kinetic energy during the time the particle slips (just after impact to just before beginning pure rolling motion),

$$\Delta E = E_k^{i} - E_k^{f}.$$

We average $\Delta E/E_f^{i}$ over the impact parameter $b(0 \leqslant b \leqslant 2a$, where $a=d/2)$ and the collision angle γ $(\pi/2 < \gamma \leqslant \pi)$ which is the angle between $\hat{n}$ and $\vec{v}_c$ (relative velocity at the point of contact). In this calculation (i) we used the same coordinate system as that used to compute the binary collision rule, (ii) the motion of the particles is constrained to a plane, so the components of the dynamical variables perpendicular to the plane of motion were neglected, and (iii) for ease of calculation, we assume the particle(s) to be rolling before suffering a collision.

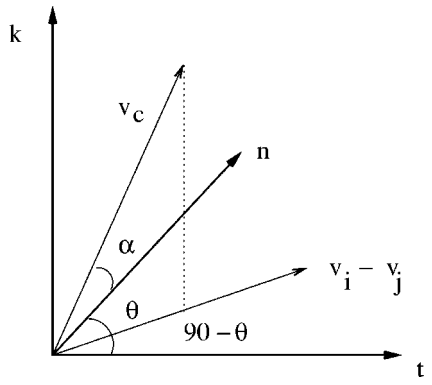

FIG. 20. A schematic diagram of the set of axes used to carry out the collisional dynamics calculation and the calculations shown in this section. The colliding particle dynamical variables $\vec{v}_c$ and $\vec{v}_i - \vec{v}_j$ are shown in the diagram.

Using Fig. 20 and the impact parameter $\vec{b}$,

$$\vec{b} = (\vec{r}_i - \vec{r}_j) \times \frac{(\vec{v}_i - \vec{v}_j)}{|\vec{v}_i - \vec{v}_j|},$$

we obtain the following expressions for $\Delta E/E_f^{i}$: (1) For particle-particle collisions,

$$\frac{\Delta E}{E_f^{i}}_{ppc} = \frac{F(b,\gamma,\alpha,\beta)}{G(b,\gamma,\alpha,\beta)}, \tag{A7}$$

where $F(b,\gamma,\alpha,\beta)$ and $G(b,\gamma,\alpha,\beta)$ are

$$F(b,\gamma,\alpha,\beta) = \frac{1}{7}\left[({c_1}^2 - c^2)\cos^2\gamma + ({c_2}^2 - {c_1}^2)\cos^2\gamma\left(\frac{b}{2a}\right)^2 - c^2\left(\frac{b}{2a}\right)^2 + c^2 \right], \tag{A8}$$

$$G(b,\gamma,\alpha,\beta) = \left[\frac{1+q}{2} + q\left(\frac{c^2}{2} - c\right)\right]\left[1 - \left(\frac{b}{2a}\right)^2\right] + \left[\left(\frac{{c_1}^2}{2} - c_1\right) - q\left(\frac{c^2}{2} - c\right)\right]\cos^2\gamma + \left[-\left(\frac{{c_1}^2}{2} - c_1\right) + \left(\frac{{c_2}^2}{2} - c_2\right)\right]\cos^2\gamma\left(\frac{b}{2a}\right)^2. \tag{A9}$$

Here,

$$c_1 = 1 + \alpha,$$

$$c_2 = q\frac{1+\beta}{1+q},$$

$$c = \frac{1+\beta}{2(1+q)}.$$

For particle-wall impacts (see Fig. 20),

$$\frac{\Delta E}{E_f^i}_{pwc} = \frac{P(b,\theta,\alpha,\beta)}{Q(b,\theta,\alpha,\beta)}, \tag{A10}$$

where $P(b,\theta,\alpha,\beta)$ and $Q(b,\theta,\alpha,\beta)$ are

$$P(b,\theta,\alpha,\beta) = \frac{14}{49}[(c_3 - c_1)^2 \sin^2\theta + c_2{}^2 \cos^2\theta], \tag{A11}$$

$$Q(b,\theta,\alpha,\beta) = \left[(1-c_1)^2 + \frac{2}{5}(1-c_3)^2\right]\sin^2\theta + \left[(1-c_2)^2 + \frac{2}{5}\right]\cos^2\theta, \tag{A12}$$

and where

$$c_1 = 1 + \alpha,$$

$$c_2 = q\frac{1+\beta}{1+q},$$

$$c_3 = \frac{1+\beta}{1+q}.$$

Tables I and II, respectively, summarize results for special cases of collisions between particles and between particles and the wall.

[1] H.M. Jaeger, S.R. Nagel, and R.P. Behringer, Rev. Mod. Phys. **68**, 1259 (1996).
[2] B. Painter and R.P. Behringer, Phys. Rev. Lett. **85**, 3396 (2000).
[3] B. Painter and R.P. Behringer, Phys. Rev. E **62**, 2380 (2000).
[4] B. Painter, M. Dutt, and R.P. Behringer, Physica D **175**, 43 (2003).
[5] J.S. Olafsen and J.S. Urbach, Phys. Rev. Lett. **81**, 4369 (1998).
[6] J.S. Olafsen and J.S. Urbach, Phys. Rev. E **60**, R2468 (1999).
[7] A. Kudrolli, M. Wolpert, and J.P. Gollub, Phys. Rev. Lett. **78**, 1383 (1997).
[8] A. Kudrolli and J. Henry, Phys. Rev. E **62**, R1489 (2000).
[9] F. Melo, P. Umbanhowar, and H.L. Swinney, Phys. Rev. Lett. **72**, 172 (1994).
[10] F. Melo, P. Umbanhowar, and H.L. Swinney, Phys. Rev. Lett. **75**, 3838 (1995).
[11] D.K. Mueth *et al.*, Phys. Rev. E **57**, 3164 (1998); B.J. Miller, C. O'Hern, and R.P. Behringer, Phys. Rev. Lett. **77**, 3110 (1996).
[12] D. Howell, C. Veje, and R.P. Behringer, Phys. Rev. Lett. **82**, 5241 (1999); Phys. Rev. E **59**, 739 (1999); Chaos **9**, 599 (1999).
[13] A. Domenech, T. Domenech, and J. Cebrian, Am. J. Phys. **55**, 231 (1987).
[14] W. Losert, D.G.W. Cooper, J. Delour, A. Kudrolli, and J.P. Gollub, Chaos **9**, 682 (1999).
[15] J.S. Urbach and J.S. Olafsen, in *Granular Gases*, edited by T. Pöschel and S. Luding (Springer, Berlin, 2001).
[16] J. Witters and D. Duymelinck, Am. J. Phys. **54**, 80 (1986).
[17] S.F. Foerster, M.Y. Louge, H. Chang, and K. Allia, Phys. Fluids **6**, 1108 (1994).
[18] F. Radjai and S. Roux, Phys. Rev. E **51**, 6177 (1995).
[19] D.E. Wolf, in *Computational Physics Selected Methods—Simple Exercises—Serious Applications*, edited by K.H. Hoffmann and M. Schreiber (Springer, Heidelberg, 1996).
[20] S. McNamara and S. Luding, Phys. Rev. E **58**, 813 (1998).
[21] J. Gersten, H. Soodak, and M.S. Tiersten, Am. J. Phys. **60**, 43 (1992).
[22] S. Luding, Phys. Rev. E **52**, 4442 (1995).
[23] L. Kondic, Phys. Rev. E **60**, 751 (1999).
[24] S. Luding, in *Physics of Dry Granular Media*, edited by H.J. Herrmann, J.-P. Hovi, and S. Luding (Kluwer Academic, Dordrecht, 1998), p. 285.
[25] S. Luding and H.J. Hermann, Chaos **9**, 673 (1999).
[26] I. Goldhirsch, Chaos **9**, 659 (1999).
[27] I. Goldhirsch, M.-L. Tan, and G. Zanetti, J. Phys.: Condens. Matter **8**, 1 (1993).
[28] J. Walker, Sci. Am. **249**, 124 (1983).
[29] R.E. Wallace and M.C. Schroeder, Am. J. Phys. **56**, 815 (1988).
[30] G. Kuwabara and K. Kono, Jpn. J. Appl. Phys., Part 1 **26**, 1230 (1987).
[31] I. Goldhirsch and G. Zanetti, Phys. Rev. Lett. **70**, 1619 (1993).
[32] P.A. Thompson and G.S. Grest, Phys. Rev. Lett. **67**, 1751 (1991).
[33] L.E. Silbert, D. Ertaş, G.S. Grest, T.C. Halsey, D. Levine, and S.J. Plimpton, Phys. Rev. E **64**, 051302 (2001).
[34] L.E. Silbert, G.S. Grest, S.J. Plimpton, and D. Levine, Phys. Fluids **14**, 2637 (2002).
[35] P. Zamankhan *et al.*, Phys. Rev. E **60**, 7149 (1999).
[36] S. Goyal, A. Ruina, and J.M. Papadopaulos, Wear **143**, 307 (1991).
[37] S. Goyal, A. Ruina, and J.M. Papadopaulos, Wear **143**, 331 (1991).
[38] Z. Farkas, G. Bartels, T. Unger, and D.E. Wolf, Phys. Rev. Lett. **90**, 248302 (2003).
[39] M.P. Allen and D.J. Tildesley, *Computer Simulation of Liquids* (Oxford University Press, New York, 1987).
[40] M. Dutt and R.P. Behringer (unpublished).